RSC Advances

PAPER

View Article Online
View Journal | View Issue

Cite this: *RSC Adv.*, 2026, **16**, 11496

Sustainable antibacterial nanocoating from polycaprolactone grafted with dapsone and silver nanoparticles for boosting the properties of bagasse paperboard for active food packaging

Hesham Moustafa, *[ab] Fatehy M. Abdel-Haleem[c] and Mohamed H. Hemida[d]

Nanocoating technology for by-product bagasse papers (BPs) utilizes hybrid polymers to create a superhydrophobic surface that enhances several properties of the BP material, which is highly promising for many applications, including active food packaging. Thus, this study aimed to prepare a functional nanocoating from polycaprolactone (PCL) grafted with dapsone (DAP) and silver nanoparticles (Ag NPs) for promoting the properties of hydrophilic BPs. The outcome of grafting DAP into PCL, as well as the interactions between the components after the coating process, were investigated by FT-IR and XRD analyses. Varied contents of the Ag NPs (*i.e.*, 0.05%, 0.15%, and 0.30%) were used to fabricate a PCL-DAP–Ag nanocoating for treating the hydrophilic BPs using a dip-coating approach. The net-treated BPs (TBPs) were subjected to various analyses and tests, including morphological tests by XRD and SEM analyses, mechanical and barrier property evaluation, wettability assessment by the water contact angle (WCA), flammability resistance testing, and antibacterial activity measurements. The results revealed that most of the properties of the TBPs were further enhanced by the presence of Ag NPs, especially at 0.15%, compared to raw BP or unfilled TBP. The flammability resistance of TBP-0.30% Ag was achieved when the Ag NP content in the nanocoating reached 0.30%. Moreover, the treated BPs demonstrated superior antibacterial activity, which effectively killed microbes and inhibited their growth within an inhibitory zone ranging from 14 to 33 mm, depending on the microbe and sample type. In summary, PCL grafting is influential, and applying PCL-DAP-based Ag NPs as a nanocoating to hydrophilic BPs presents a highly promising strategy for antimicrobial food packaging applications.

Received 20th January 2026
Accepted 17th February 2026

DOI: 10.1039/d6ra00530f

rsc.li/rsc-advances

1. Introduction

Sugarcane bagasse (SCB) is an agricultural waste produced in large quantities worldwide from the cash crop sugarcane industry. It is estimated that the amount of SCB produced annually reaches 0.6 billion tons.[1] Several years ago, a significant amount of SCB was lost through burning or disposal in wastelands, which contributed to numerous environmental problems, including climate change. However, chemical engineering and industrial biotechnology have employed thermal, chemical, and biological valorization methods to obtain new and valuable materials from SCB, thereby demonstrating the sustainability of SCB.[2] SCB has been improved for use in the production of enzymes, nanocellulose, organic acids, biofuels, biogas, paper pulp, and syngas; in bio-composites by blending with plastics, biochar, animal feed, food packaging; and as environmental adsorbents for the removal of pollutants from air and wastewater.[1,3] Other studies[4,5] have reported the use of the ash of SCB as an additional cementitious material to boost the properties of concrete. Moreover, bagasse papers (BPs) are an important sustainable product of SCB, as it is a good feedstock that replaces wood for producing paper pulp without the need for deforestation.[1,6] SCB is rich in cellulose (~50 wt%), hemicellulose (~25 wt%), lignin (~24 wt%), and other trace compounds; cellulosic fibres are the most important component during paper pulp production, whereas other SCB components are removed by hammer mills and chemical pulping through the kraft process. Bio-pulping using microorganisms is preferred to chemical pulping because of its environmental friendliness and cost-effectiveness.[1,6,7] BPs are used in various applications, including intelligent, see-through, ultraviolet-resistant, and antimicrobial packaging because

[a]*Chemical Metrology Division, National Institute of Standards (NIS), Tersa Street, El Haram, P. O. Box 136, Giza 12211, Egypt. E-mail: hesham.moustafa21@gmail.com*
[b]*Bioanalysis Laboratory, National Institute of Standards (NIS), Tersa Street, El Haram, P. O. Box 136, Giza, 12211, Egypt*
[c]*Department of Chemistry, College of Science, Imam Mohammad Ibn Saud Islamic University (IMSIU), Riyadh, 11623, Saudi Arabia*
[d]*Department of Agricultural Engineering, Faculty of Agriculture, Cairo University, Giza, Egypt*

they are cost-effective, non-toxic, eco-friendly, and biodegradable.[3] Nevertheless, the key disadvantage of BPs in food packaging is their hydrophilicity and permeability properties, which restrict their marketability as a substrate or reinforcing material in polymer matrices. Thus, it has been reported that the hydrophobicity and other properties of BPs are improved by coating using sustainable polymers, namely, polycaprolactone (PCL).

PCL is an eco-friendly and biodegradable polymer that is used in food packaging owing to its unique properties, including excellent water resistance resulting from its hydrophobicity, ease of modification and derivatization, biocompatibility, flexibility, and thermoplasticity. In addition to the high quality of PCL, coating BP with this hydrophobic biopolymer extends the shelf life of food as long as possible. However, the mechanical stiffness, antimicrobial activity, and flammability resistance of PCL are major problems, in addition to its high price. Several studies[8–10] have been performed to further enhance the properties of PCL in order to overcome these deficiencies, either by blending with other copolymers, copolymerization with certain monomers, or by incorporation with nanoparticles. In some cases, studies have used functional or grafting agent-based antimicrobial components, which is the most common and efficient procedure, not only for enhancing the properties of PCL, including biocompatibility, when used as a nanocoating with hydrophilic BP, but also for use in a broader range of applications;[11–13] DAP is used as a grafting agent in this work. DAP is an antibiotic that belongs to the sulfonamide family of medicines; it is highly effective against the growth of different microbes.[14,15] Owing to its structural feature, it is used as a grafting agent in certain polymers.[16,17] Accordingly, different derivatives of DAP have been prepared and studied for their use as antimicrobial materials in active food packaging processes, without harmful effects to humans.[14,18]

Antimicrobial food packaging, a specific type of active packaging, refers to the use of antimicrobial agents to inhibit microbial growth.[19–21] Active food packaging includes the use of antioxidants, antimicrobials, gas controllers, or light blockers to get rid of environmental factors that may rapidly cause food damage, such as humidity, temperature, oxygen, or other gaseous species. However, antimicrobial food packaging is not only concerned with harmful microbes but also with improving mechanical strength, as packaging materials with poor mechanical strength may significantly affect food quality, shelf life, or safety during handling, transportation, or storage.[20,21] To fulfill that, different nanomaterials have been incorporated into biopolymers and reported in the existing literature,[19,20,22–24] not limited to silver nanoparticles (Ag NPs), composites of Zn–cellulose, chitosan–TiO_2, cellulose–TiO_2, expanded organoclay, and ZnO–SiO_2. However, Ag NPs is a superior material because of its ease of preparation, cost-effectiveness, high efficiency at sublethal concentrations due to its high surface-to-volume ratio, antioxidant activity, flammability resistance, and sustained preservation action due to its slow release during food packaging interaction. Furthermore, it exhibits a wide range of antimicrobial activity against more than 60 types of microbes and can absorb humidity and fluids of meat and fish, keeping food packaging attractive.[3,19–22,25,26] Ag NPs were reported to be composited and incorporated within a polymer or fiber network to form an effective food packaging composite;[3,7,19,20] gum–silver, polyvinyl alcohol–nanocellulose–silver, and cellulose nanofibril–silver were reported for this purpose.[24,27–30] To increase the antimicrobial activity and avoid the agglomeration of Ag NPs within the fiber or polymer network, it can be composited with other species, such as graphene oxide and nanocellulose.[3,28]

In this work, PCL was grafted with dapsone, followed by the embedment of Ag NPs to be used as a sustainable nanocoating for improving the properties of hydrophilic BPs, including mechanical strength, barrier performance, hydrophobicity, flammability resistance, and antimicrobial activity. The proposed material can be applied in biodegradable food packaging applications.

2. Materials and methods

2.1. Materials

PCL bioplastic in beads ($M_w \sim 80\,000$) was offered by Thermo Fisher Scientific Co. (USA). Bagasse paperboard-based sugarcane waste (BPs) was obtained from Quena Paper Industry Co. (Egypt) and utilized as a substrate. DAP (purity = 98%) was used as a functionalized material and supplied by Alfa Aesar, Kandel (Germany). Silver nitrate ($AgNO_3$) and sodium borohydride ($NaBH_4$), which were used to prepare the Ag NPs, as well as tetrahydrofuran (THF, 99.9%), were bought from Sigma-Aldrich (Egypt). Briefly, 0.190 g of $AgNO_3$ was dispersed in 100 mL of deionized water (DIW) and agitated under magnetic stirring for ~6 min. Then, 1.62 mL of $NaBH_4$ (0.0076%) was added dropwise to the aforementioned solution under vigorous stirring for an additional 15 min. The admixture was kept in an ice bath and then exposed to UV irradiation (UVP CL 1000, light lamps (λ = 365 nm)) for ~10 min to complete the reaction. The reaction was completed when the mixture turned yellow, confirming the formation of Ag NPs. Thereafter, the particle size distribution and zeta potential of the synthesized Ag NPs were verified using a Malvern Zetasizer. Fig. 1(a and b) shows that the average particle size distribution was in the range of ~29–34 nm, and their zeta potential was approximately -35.10 ± 7.3 mV, suggesting the good stability of the nanoparticles in an aqueous solution. The powder was then stored in a dark bottle for further experiments.

2.2. Preparation of PCL-DAP and its nanocoating

The preparation of PCL-DAP was performed using an *in situ* route (Fig. 2) as follows: 1.5 g of PCL was placed in a two-neck round flask containing 50 mL of THF under magnetic stirring. When the polymer was completely dissolved, 0.25 g of DAP was added to the PCL solution, and the mixture was then refluxed at 65 °C overnight with continuous stirring. The mixture was cooled under normal conditions and then sonicated (amplitude = 60%) for 15 min, while maintaining the regime in an ice bath to prevent overheating and obtain a functionalized PCL-DAP matrix. Subsequently, three different ratios of the Ag NPs (*i.e.*,

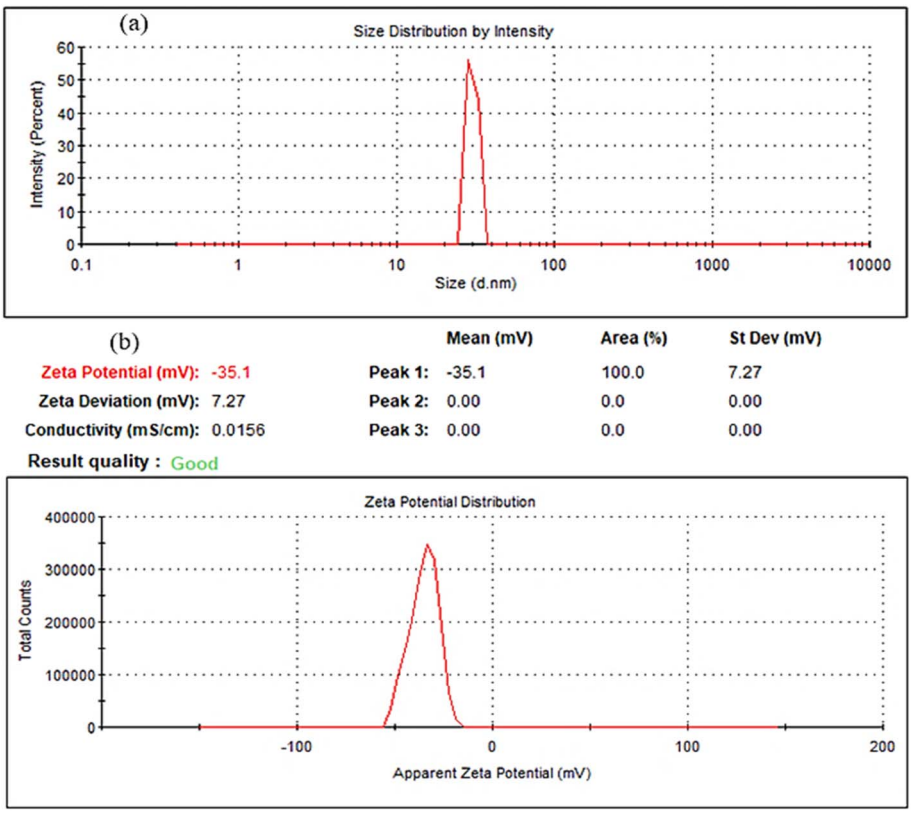

Fig. 1 (a) Particle size distribution and (b) zeta potential of the prepared Ag NPs.

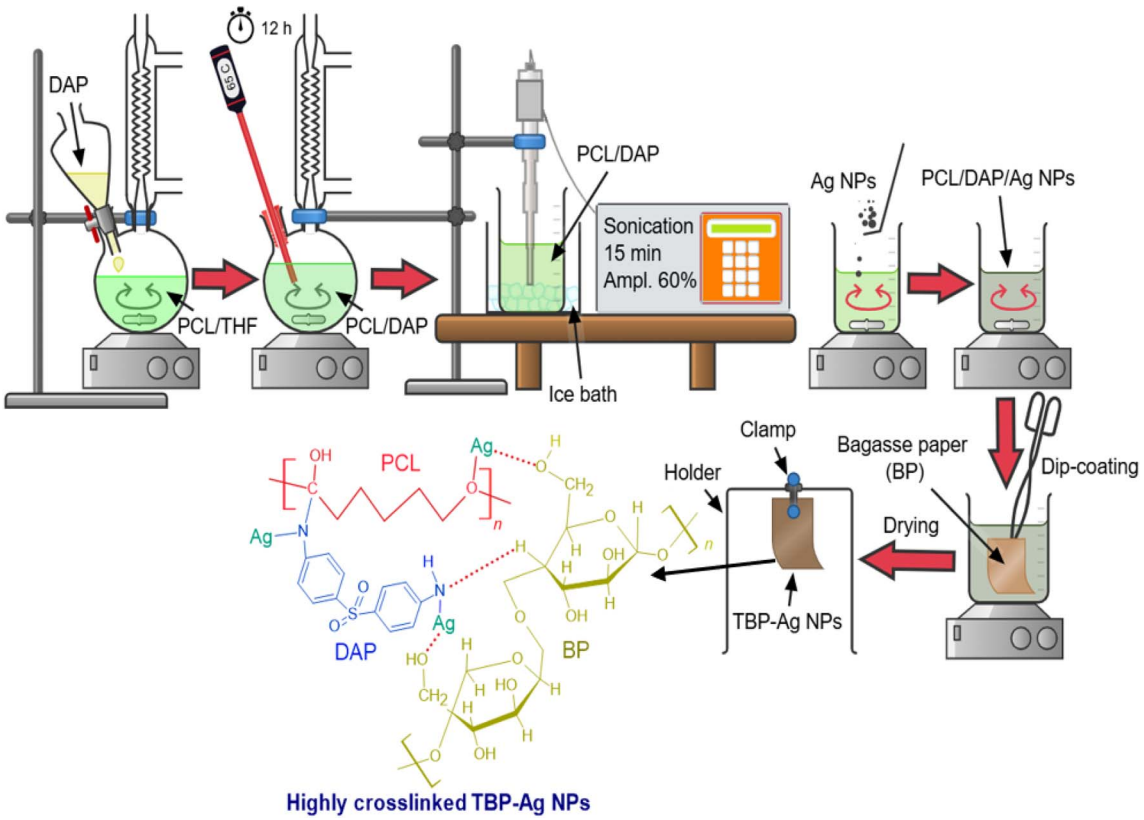

Fig. 2 Preparation steps for PCL-DAP and its nanocoating with Ag NPs as well as the dip-coating of TBP.

0.05, 0.15, and 0.30%) were used and separately mixed with the PCL-DAP solution. For the coating of BPs, a dip-coating approach, as shown in Fig. 2, was applied by dipping the BPs in the nanocomposite mixture for 10 min and removing them to dry in a normal climate. The treated BPs were labelled according to the Ag NP content in the nanocomposite mixture as TBP (BP-PCL-DAP), TBP-0.05 Ag (BP-PCL-DAP–0.05 Ag NPs), TBP-0.15 Ag (BP-PCL-DAP–0.15 Ag NPs), and TBP-0.3 Ag (BP-PCL-DAP–0.3 Ag NPs). Additionally, the raw BP was utilized as a reference.

2.3. XRD and FT-IR spectra

An X-ray diffraction system (Bruker-AXS D8 Ascertain Diffractometer, Co Kα basis) equipped with a monochromator Cu Kα radiation (35 kV, 30 mA, and $\lambda = 1.15418$ Å) was used to investigate the structure of raw BP, pure DAP, TBP, and TBP with varying quantities of Ag NPs. The data were verified over a 2θ range from 5 to 80° with a step size of 0.05 and at a sampling width of 0.010°.[31] Also, the functional properties of the treated BP sheets with the PCL-DAP–Ag nanocoating were characterized using a PerkinElmer Spectrum 100 FT-IR spectrometer in the ATR mode. The spectral range for all the specimens was 4000 to 400 cm^{-1} with a resolution of 4 cm^{-1}, and 64 scans were conducted to capture the spectra.

2.4. SEM analysis

The surface topography and dispersibility of Ag NPs for all the specimens were investigated *via* scanning electron microscopy (SEM, QUANTA 3D 200i). The prepared specimens were coated with a thin carbon layer using a sputter coater 108carbon/A before the examination to avoid any electrostatic charging during the visualization. The acceleration voltage was in the range of 5–10 kV.[32]

2.5. Mechanical testing

The mechanical properties were measured using an Instron 34SC-5 Universal Tensile testing machine (UK), with a load cell of 5 kN and a crosshead speed of 50 mm min^{-1} at a temperature of 23 ± 2 °C and relative humidity (RH 50 ± 5%), complying with ISO 1924-2. The mean value was taken from three parallel trials for each sheet.

2.6. Barrier properties

The water vapor transmission (WVT) for the treated BPs was evaluated using a desiccant procedure in accordance with the ASTM E96 standard, as detailed in our previous study.[33] Briefly, the samples were excised from the treated BP sheets into a 30 mm ring shape and mounted in the assemblies containing approximately 10 g of $CaCl_2$, which was pre-dried at 105 °C for 6 h before testing. The initial weight of each assembly was recorded before placement in a climate chamber maintained at 23 ± 1 °C and 50% ± 5% relative humidity (RH). The assembly weights were recorded regularly every 12 h interval until a steady state mass was reached, typically over a period of 10 days. Throughout the experiment, the mass uptake of $CaCl_2$ was monitored as an indicator of water vapor ingress. The WVT values were then calculated as a function of the water vapor permeability coefficient (WVP) for each sample using the following equations:[33]

$$\mathrm{WVP} = \frac{\mathrm{WVT} \times L}{S(R_1 - R_2)}, \quad (1)$$

$$\mathrm{WVP} = \frac{W}{t \times A}, \quad (2)$$

where L is the BP sheet thickness (m), S is the water vapor pressure at saturation (Pa) and is equal to 133.3 Pa at 20 °C,[33] R_1 and R_2 are the relative air humidities at each surface of the sample (*i.e.*, equal 1 to 0.22, respectively), WVP is the water vapor transmission rate (g h^{-1} m^{-2}), W is the weight change, t is the time (s), and A is the exposed area for permeation (m^2). Duplicates for each BP sheet were produced, and their mean value was recorded.

2.7. Wettability measurements

The wettability in terms of the water contact angle (WCA) for all the samples was measured by depositing various water droplets on the surface of the specimens using a Theta Optical Tensiometer (model: OAC 13EC, Germany), which is equipped with a programmed camera. The WCA values were obtained after the deposition during the first few seconds using ImageJ software, and the mean value was taken from at least three trials for each specimen.

2.8. Flammability test

The UL 94 vertical burning flame chamber, established at Heliopolis Company for Chemical Industries (Egypt), was employed to assess the impact of the BP sheets treated by nanocoating (PCL-DAP–Ag NPs) on the flammability properties of the coated samples, in accordance with the ASTM D6413-15 test method. The specimens were placed between the holder clamps, fixed, and exposed to the burner, which was 35 mm in height, for 10 ± 0.3 s. The after-flame time (t_{af}, s) was evaluated. At least three replicates for each treated BP sheet were measured, and the mean was recorded.

2.9. Antibacterial assays

The CompactDry™ TCR agar diffusion disks (Nissui Pharmaceutical Co., Japan) were used as vegetated media for *Staphylococcus aureus* (*S. aureus*, G^{+ve} bacteria) and *Escherichia coli* (*E. coli*, G^{-ve} bacteria). Both bacteria were separately spread on the media using the agar disk-diffusion method. The treated TBP specimens were dried in a normal climate under sterilized conditions before the test. Next, the specimens were placed on top of the media surface seeded with selected microbes, followed by incubation for 24 h at 37 °C.[34] The bacteria were cultivated surrounding the specimen after the incubation time, and then the inhibition zone diameter (IZD) was calculated and is expressed in millimeters (mm).

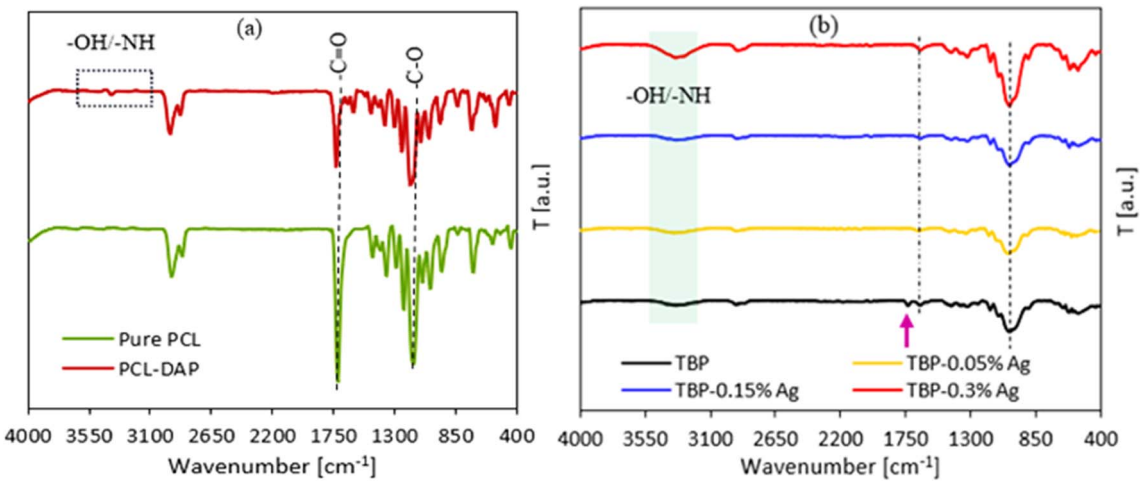

Fig. 3 (a) FT-IR spectra recorded in the ATR mode for pure PCL and PCL-DAP. (b) FT-IR spectra of TBP and its nanocoating with different quantities of Ag NPs.

3. Results and discussion

3.1. FT-IR analysis

Fig. 3(b) shows the FT-IR spectra of pure PCL and its functionalization with DAP. The FT-IR spectra of PCL typically demonstrated the main absorption peaks at ~2954 cm^{-1} and 2870 cm^{-1}, assigned to symmetric and asymmetric $-CH_3$ and $-CH_2$, respectively. Other sharp absorption peaks were located at ~1716 cm^{-1} and ~1155 cm^{-1}, attributed to the carbonyl group (–C=O) and –C–O groups, respectively.[35,36] For PCL-DAP, new absorption peaks were observed at ~3382–3215 cm^{-1}, corresponding to the –OH and –NH groups. Meanwhile, the reduction of the –C=O and –C–O peaks after the functionalization process was observed.[37] Additionally, both peaks were shifted to higher wavenumbers, indicating the formation of –C–N (*i.e.*, appearing at ~1180 cm^{-1}). All of them evidenced the functionalization of PCL by DAP, as showcased in Fig. 2. This result was supported by the XRD spectra. The FT-IR spectra, as illustrated in Fig. 3(b), revealed interesting insights about the effect of nanocoating with varied amounts of Ag NPs on the raw BP sheets. It was found that the major absorption peaks for TBP at ~3380–3260, 2930, 2851, 1720, and 1045 cm^{-1} were attributed to the –OH/–NH stretching, symmetric and asymmetric hydrocarbons, carbonyl group, and –C–O, respectively, confirming the existence of PCL-DAP on the BP. By adding Ag NPs to PCL-DAP as a nanocoating, the intensities of the characteristic peaks appearing at 3380–3260 cm^{-1} (assigned to –OH/–NH groups) and 1045 cm^{-1} (–C–O/–C–N) increased, especially for the nanocoating containing 0.3% of Ag NPs. Meanwhile, the disappearance of the –C=O peak was observed after the addition of Ag NPs. All of these confirmed that the chemical interactions of Ag NPs inside the PCL-DAP matrix, as a nanocoating onto the BP surface, were achieved.

3.2. X-ray diffraction

Fig. 4(a and b) shows the XRD patterns for TBP and its nanocoating with varying amounts of Ag NPs (*i.e.*, 0.05 to 0.3 wt%)

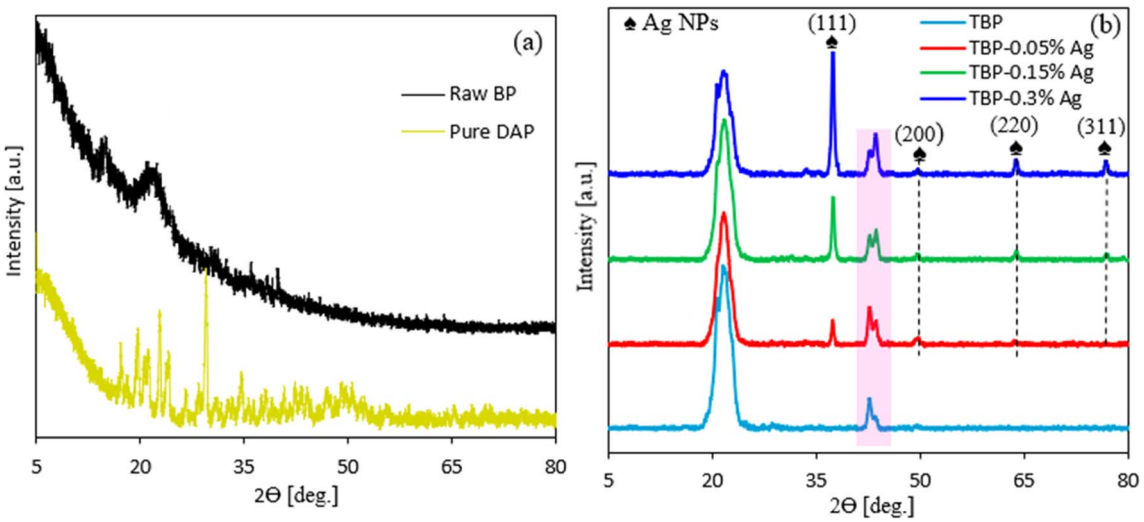

Fig. 4 (a) XRD patterns for raw BP and pure DAP as well as for TBP without and with varying contents of Ag NPs (b).

using a 2θ scanning range of 5–80°. Also, the XRD patterns of raw BP and pure DAP were provided for comparison. Fig. 4(a) shows that sharp peaks with varying intensities appeared for pure DAP, suggesting its crystalline structure. However, the majority of these peaks disappeared when DAP reacted with PCL (Fig. 4(b)). Furthermore, the XRD pattern for the treated TBP typically exhibited a prominent diffraction peak at 2θ = 20°–21.95°, corresponding to the (110) plane, which splits into two peaks attributed to BP, PCL, and DAP, indicating their amorphous, semi-crystalline, and crystalline structures, respectively.[16,38] Moreover, a new diffraction peak appeared at $2\theta \sim 42.8°$, which was absent in both neat PCL[38] or pure DAP, and attributed to PCL-DAP, confirming the successful functionalization of PCL by DAP (Fig. 2). Upon incorporating Ag NPs into PCL-DAP to form the nanocoating, additional sharp diffraction peaks appeared at $2\theta \sim 37.45°$, 49.68°, 63.95°, and 76.88°, corresponding to the (111), (200), (220), and (311) crystallographic planes of Ag NPs in the nanocoating.[39] The intensities of these peaks increased with an increase in the Ag NP content in the matrix (Fig. 4(b)), suggesting better compatibility and the nano dispersion of Ag NPs onto the BP sheets. This outcome aligns with a previous report.[39]

3.3. SEM analysis

SEM images can reveal interesting data about the morphology of the nanocoating and the dispersion quality of Ag NPs on the BP surface, as shown in Fig. 5. The micrograph for the TBP sheet showed poor interfacial bonding with voids and empty spaces, which were attributed to the challenge between the hydrophilic nature of BPs and the hydrophobicity of the polymer matrix. By adding 0.05% or 0.15% of Ag NPs into the PCL-DAP matrix, better biocompatibility and nanofiller dispersion throughout the matrix, with the absence of voids and empty spaces, were observed. This was apparently due to the presence of Ag NPs, which contributed as a coupling agent to create interfacial bonds between the BP surface and nanocoating matrix (Fig. 2), thereby achieving compatibility. In addition to their filling character, which agreed with the particle size assessment using the Zetasizer apparatus, to be within the range of 29–34 nm (Fig. 1). However, when augmenting the Ag NP ratio (*i.e.*, 0.3%), a phase separation (incompatibility) with a rough surface was noticed compared to the other nanocoating matrices (*i.e.*, 0.5% and 0.15%). This was ascribed to the nanofiller aggregation, which induced poor cohesion between the cellulosic groups of the BP sheet and the nanocoating matrix. This outcome absolutely agreed with that reported for the mechanical and barrier properties.

3.4. Mechanical testing

Considering the packaging-based coating, the mechanical properties played a crucial role in mitigating the predicted risk associated with the packaging substance during storage, transportation, and handling, thereby leading to an extended product shelf-life. Consequently, the tensile properties were investigated to explore the impact of the nanocoating containing different proportions of Ag NPs (*i.e.*, 0.05%, 0.15%, and 0.3%) on the properties of the TBPs. Fig. 6 presents the findings. The raw BP was also investigated for comparison; it had a tensile strength of 30.9 MPa with a strain at break of 1.4%. With the coating of the BP by PCL-DAP, both mechanical

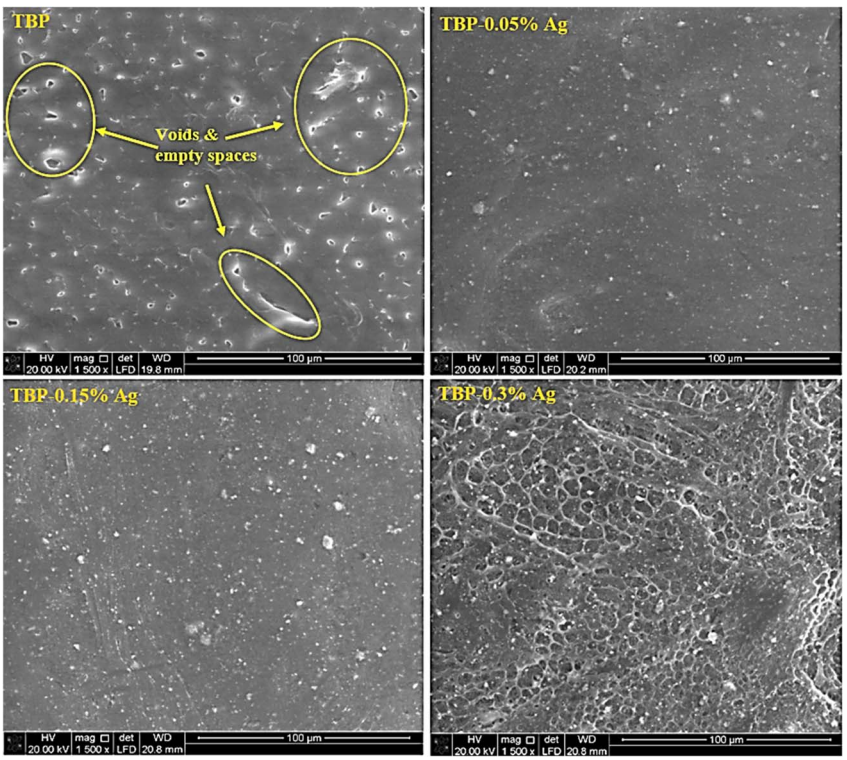

Fig. 5 SEM images of TBP and its nanocoating matrices at a magnification of 1500×.

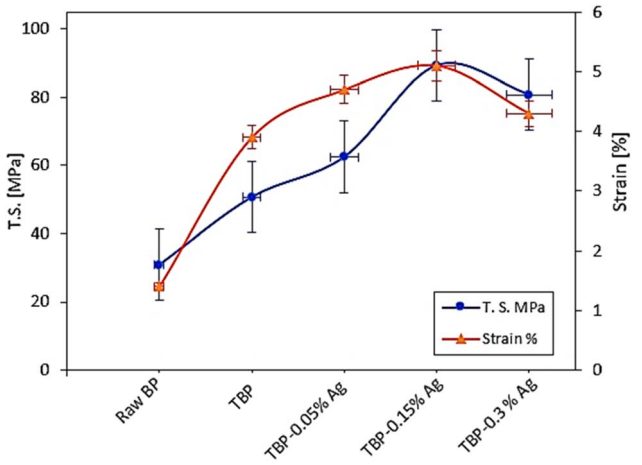

Fig. 6 Tensile properties of raw BP, TBP, and other samples with different ratios of Ag NPs.

parameters increased to ~50.7 MPa and 3.9%, respectively. Furthermore, when the BP sheets were coated with nanocomposites, an abrupt change in strength and strain occurred by increasing the ratio of the Ag NPs up to 0.15% in the nanocomposite, and their values reached ~89.3 MPa and 5.1%, respectively. This enhancement was apparently due to the reinforcing impact of inorganic Ag NPs, which provided better compatibility between the surface of the BP and the functional sites in the nanocomposite. However, both tensile parameters were reduced to ~80.8 MPa and 4.3%, but their values are still higher than those for the raw BP (*i.e.*, 30.9 MPa and 1.4%, respectively). This reduction was probably due to nanofiller aggregates, which led to the interfacial debonding between the cellulose of BP and the functional sites in the nanocomposite matrix. In summary, the coated BPs are, therefore, recommended for use in a variety of potential applications, including food packaging, with an Ag NP content of up to 0.15%.

3.5. Barrier properties

The WVP property is considered to be of utmost importance for green packaging applications because the penetration of humidity into foodstuffs through the packaging material accelerates their decay. An experiment was conducted using a desiccant procedure at 23 °C and 50% RH for 10 days. The WVP values for the treated BPs were comparable to those of the raw BP sample, as reported in Table 1. As shown in the table, the raw BP exhibited a higher WVP value, reaching ~6.80 g m^{-1} s^{-1} Pa^{-1}, indicating its hydrophilic nature. By dipping the BP in the PCL-DAP matrix, the WVP of the TBP sheet was reduced to 2.50 g m^{-1} s^{-1} Pa^{-1}, suggesting the hydrophobic nature of the functionalized polymer. However, the barrier property can be influenced by certain parameters like the shape and type of the reinforcing material, as well as the compatibility and nanofiller distribution, in addition to the crystallinity of the material.[40] Thus, with the further treatment of BP by a nanocomposite containing 0.15% Ag NPs, a significant decrease in the WVP barrier property was noticed, and its value reached 0.95 g m^{-1} s^{-1} Pa^{-1} compared to those of other matrices, indicating high barrier properties. The enhancement was attributed to the insertion of Ag NPs into the polymer matrix, indicating improved compatibility and distribution quality of the nanofiller throughout the entire polymer matrix.[41] This process ensures the establishment of crosslinked networks through covalent and hydrogen bonds (Fig. 2), thereby enhancing the barrier properties. Nevertheless, when the concentration of Ag NPs increased to 0.3%, the WVP value began to increase because of the compact nanofiller aggregates, causing decohesion and phase separation between the cellulose BP and coating nanocomposite. This creates a preferential pathway for moisture molecules within the coated BP. This result aligns with that obtained *via* the SEM observations and tensile tests.

Table 1 Barrier properties for treated BP samples compared to raw BP

Sample code	WVP (10^{-12} g m^{-1} s^{-1} Pa^{-1})
Raw BP	6.80 ± 1.45
TBP	2.50 ± 0.94
TBP-0.05% Ag	1.76 ± 0.86
TBP-0.15% Ag	0.95 ± 0.18
TBP-0.3% Ag	1.35 ± 0.75

3.6. Wettability evaluation for treated BPs

Wettability or WCA measurements were conducted to check the surface properties of the treated BPs and assess the impact of the Ag NP content through the nanocomposite used in the coating process. Fig. 7 presents the WCA data, including the representative images of their measurements using distilled water as a probe solution. It was noticed that the WCA for raw BP was 49°, confirming the hydrophilic nature of the material. It increased to 77° when the BP sheet was coated by PCL-DAP, indicating the hydrophobic character of the polymer.

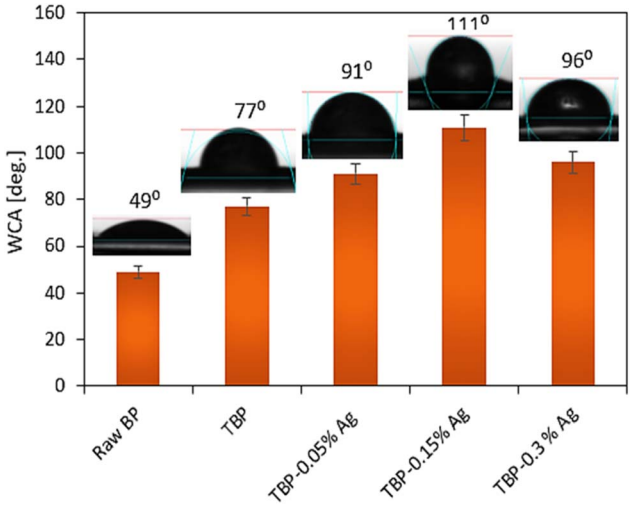

Fig. 7 WCA measurements for raw BP, TBP, and their treatments with varying concentrations of Ag NPs.

Moreover, the WCA values dramatically increased with the addition of Ag NPs to 91° and 111° for TBP-0.05% Ag and TBP-0.15% Ag, respectively, suggesting that this effect was amplified when the Ag NP amount reached 0.15% in the nanocomposite. This implied that the hydrophobicity strongly depended on the crosslinking degree of the material. In other words, the Ag NPs can link with the functional sites in the matrix and cellulose BPs, leading to more interlocking and hydrophobic material. However, with a further increment in the Ag NP content, *i.e.*, 0.3%, the WCA value reduced to 96° for TBP-0.3% Ag, indicating that an interfacial debonding occurred. These measurements align with those reported for the mechanical and barrier properties, as well as the SEM observations.

3.7. Flammability test

The flammability performance of the treated BP sheets with varying Ag NP contents was evaluated to determine their suitability for use in green packaging applications. The outcomes, summarized in Fig. 8(a), revealed that the raw BP sheet was highly flammable, exhibiting a burning rate of ~703 mm s^{-1}. When the BP sheet was coated with PCL-DAP, the burning rate reduced to 350 mm s^{-1}, suggesting that the formation of a protective layer from the complex PCL-DAP structure effectively suppressed heat transfer into the bulk of the BP. Moreover, dipping the BP sheets in nanocomposites containing different proportions of inorganic Ag NPs (*i.e.*, 0.05% to 0.3%) led to a significant reduction in the burning rate from ~164 to 46 mm s^{-1}, respectively, indicating that the burning process was substantially retarded.[42] Such achievements were apparently due to the synergistic impact between the inorganic nanoparticles and the crystallinity of the PCL-DAP polymer, which played a vital role in inhibiting heat transfer into the core of the BP during the burning process. Therefore, they were effective in delaying the flammability compared to the raw BP or TBP samples. To understand the flammability mechanism based on the dramatic decrease in the rate of burning when inorganic Ag NPs were added to the matrix, the structure of the char residue resulting from the TBP-0.3% Ag nanocoating after the flammability test was examined by FT-IR spectroscopy (Fig. 8(b)). The spectra attributed to this nanocoating before the burning were also recorded for comparison. As shown in the figure, the spectra for the char specimen revealed that some absorption peaks still existed after the burning process, such as the peaks at 2925 cm^{-1} and 2817 cm^{-1} (–CH hydrocarbons), 1708 cm^{-1} (carbonyl), and 1145–1060 cm^{-1} (C–O), indicating incomplete combustion. In addition, a broad peak appeared at the 670–534 cm^{-1} region, which can be attributed to the aromatic structure and capping of Ag NPs.[43] Thus, based on the FT-IR spectra of the char residue for the TBP-0.3 Ag NP sample, the flammability mechanism can be explained through the formation of a compact matrix, including inorganic Ag NPs and a polymer backbone, as well as the crystallinity of the TBP-0.3% Ag nanocoating (Fig. 4(b)). All of them acted as a shield layer to prevent heat transfer into the core of the material during combustion, thereby enhancing the flammability resistance.[44]

3.8. Antibacterial assay

The antibacterial activity of TBP and its treatments with varied contents of Ag NPs (*i.e.*, 0.05, 0.15, and 0.30%) was investigated to assess the developed materials for use in eco-friendly packaging applications. The assay was evaluated using two different microbes, including *S. aureus* and *E. coli*, within a contact time of 24 h and at 37 °C, as demonstrated in Fig. 9. The changes in inhibitory zones for the investigated specimens were also calculated. Fig. 9 shows that all the specimens had an inhibitory effect against both microbes used in the assay. This indicated that the biological activity of the materials had been significantly affected by the treatment process, either with PCL-DAP or the nanocoating (PCL-DAP–Ag NPs). The data suggested that the inhibitory zone ranged from 14 to 33 mm, depending on the bacteria and specimen type in the following order: TBP < TBP-0.05% Ag < TBP-0.15% Ag < TBP-0.30%. This achievement was

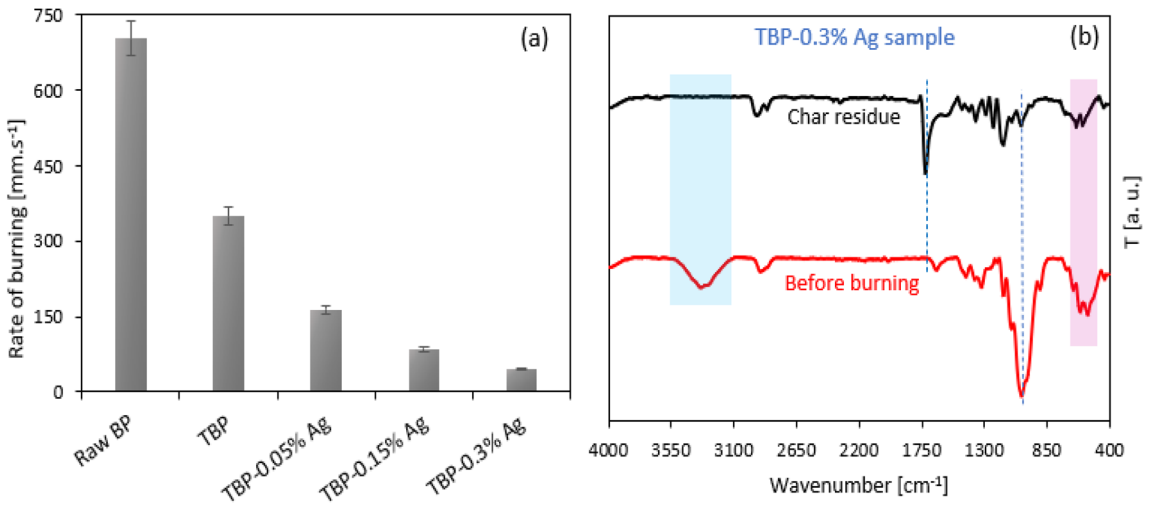

Fig. 8 (a) Burning rate data of raw BP and the treated BPs with different Ag NP contents obtained using the UL 94 chamber. (b) FT-IR spectra for the TBT-0.3% Ag specimen before and after the combustion process.

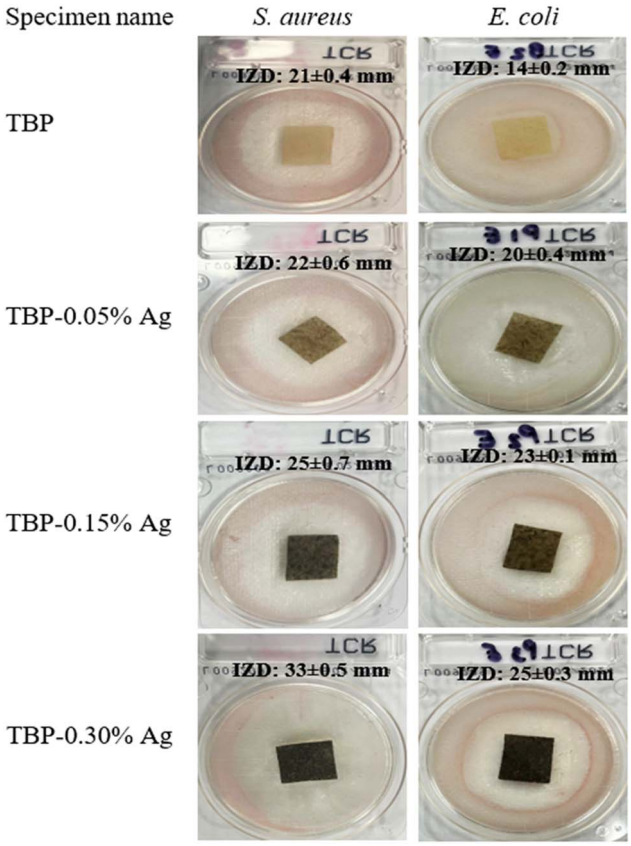

Fig. 9 Antibacterial experiments and inhibitory zones of TBP and its treatment with different ratios of Ag NPs against *S. aureus* and *E. coli* bacteria.

attributed to the presence of amino and sulfonyl (O═S═O) groups, in addition to Ag NPs, which had a superior impact in suppressing the growth of a broad spectrum of G^{+ve} and G^{-ve} bacteria. Interestingly, the figure revealed that the highest activity and efficiency against both selected bacteria were achieved by applying a higher content of Ag NPs (TBP-0.30% Ag). This can be used to draw a possible mechanism through the electrostatic attraction between the positively charged Ag NPs, combined with functional groups, and the negatively charged microbial cells, *via* the adherence of Ag^{+} to the cytoplasm and the cell wall, thereby leading to an interruption in bacterial development.[45,46]

4. Conclusions

In this research, an eco-friendly and non-toxic functional nanocoating was successfully synthesized by grafting PCL using DAP with Ag NPs to enhance the properties of hydrophilic BPs. The grafting of PCL by DAP was confirmed *via* FT-IR and XRD analyses. Three different ratios of Ag NPs (*i.e.*, 0.05, 0.15, and 0.30%) were utilized to prepare the nanocoating for modifying the hydrophilic BPs using a dip-coating procedure. The treated BPs were subjected to certain investigations, including mechanical, barrier, hydrophobicity by WCA, flammability, and antibacterial property tests. The FT-IR and XRD spectra demonstrated the chemical interactions and crystallinity of the Ag NP-based TBP sample achieved when the NP content was increased. The SEM images demonstrated better biocompatibility and a nanodispersion state between the nanocoating and treated BPs when Ag NPs were added, especially at contents of 0.05 and 0.15%. Otherwise, a high Ag NP ratio (*i.e.*, 0.30%) in the nanocoating can lead to obtain Ag aggregations.

The mechanical, barrier, and WCA property data revealed that the TBP-0.15% Ag sample was the optimal specimen and had high tensile strength ~ 89.30 MPa, WVP ~ 0.95 g m^{-1} s^{-1} Pa^{-1}, and WCA ~ 111°, compared to the unfilled TBP. Furthermore, raw BP was tested under similar conditions, and it showed strength ~ 30.90 MPa, WVP ~ 6.8 g m^{-1} s^{-1} Pa^{-1}, and WCA ~ 49°. These poor properties can, therefore, be correlated to the hydrophilic nature of BPs. A superior achievement in the flammability resistance and antibacterial properties was observed when Ag NPs were used, particularly at higher loads compared to the raw BP or unfilled TBP. The flammability resistance property represented by the rate of burning for the TBP-0.3% Ag sample was achieved and reduced to 46 mm s^{-1} compared to that of raw BP (*i.e.*, 703 mm s^{-1}) or unfilled TBP (*i.e.*, 350 mm s^{-1}). Furthermore, the treated Ag NP-based BPs demonstrated superior antibacterial activities against the selected microbes, including G^{+ve} bacteria and G^{-ve} bacteria with different diameters ranging from ~14 to 33 mm, depending on the microbe and specimen type. In summary, this work introduces a novel application of PCL grafting that proved to be highly effective. The use of PCL-DAP-based Ag NPs as a nanocoating for hydrophilic BPs showed a significant potential for antimicrobial food packaging applications.

Conflicts of interest

The authors declare that there are no conflicts of interest in this work.

Data availability

The authors confirm that the data supporting the findings of this study are available within the article.

Acknowledgements

This work was supported and funded by the Deanship of Scientific Research at Imam Mohammad Ibn Saud Islamic University (IMSIU) (grant number IMSIU-DDRSP2602).

References

1 Y. Matsueda and E. Antunes, *J. Environ. Chem. Eng.*, 2024, **12**, 114900.
2 H. Moustafa, C. Guizani, C. Dupont, V. Martin, M. Jeguirim and A. Dufresne, *ACS Sustain. Chem. Eng.*, 2017, **5**(2), 1906–1916.
3 H. Moustafa, E. M. Ahmed and M. Morsy, *Mater. Technol.*, 2022, **37**, 2766–2776.

4 A. K. Parashar and A. Gupta, *Mater. Today: Proc.*, 2021, **44**, 801–807.
5 A. Bahurudeen and M. Santhanam, *Cem. Concr. Compos.*, 2015, **56**, 32–45.
6 D. Mboowa, *Biomass Convers. Biorefin.*, 2021, **14**, 1–12.
7 A. Sharma, M. Thakur, M. Bhattacharya, T. Mandal and S. Goswami, *Biotechnol. Rep.*, 2019, **21**, e00316.
8 R. Abedi-Firoozjah, B. Bahramian, M. Tavassoli, S. Ghaderi, M. Majlesi, N. Ahmadi, S. Roy, N. Oladzadabbasabadi, H. Rajabi, M. R. Ashkezary and S. M. Jafari, *Food Bioprocess Technol.*, 2025, **18**, 9011–9051.
9 K. İlaslan and G. Tarihi, *J. Food Feed Sci. Technol.*, 2024, **32**, 13–26.
10 R. K. Arya, J. Kaur, A. Chandra, S. Ahuja, M. Rawat and J. Sharma, *J. Appl. Polym. Sci.*, 2021, **138**, 50888.
11 G. G. d'Ayala, E. Di Pace, P. Laurienzo, D. Pantalena, E. Somma and M. R. Nobile, *Eur. Polym. J.*, 2009, **45**, 3217–3229.
12 E. H. Boutriouia, T. El Assimi, H. Qayouh, M. Raihane, A. El Meziane, M. H. V. Baouab, H. Ben Youcef, A. El Kadib and M. Lahcini, *React. Funct. Polym.*, 2024, **198**, 105887.
13 T. Mohan, F. Gürer, D. Bračič, F. Lackner, C. Nagaraj, U. Maver, L. Gradišnik, M. Finšgar, R. Kargl and K. S. Kleinschek, *Biomacromolecules*, 2025, **26**, 1771–1787.
14 W. A. Al-Masoudi, T. M. Al-Tememy and R. H. Al-Assadi, *Eur. J. Chem.*, 2014, **5**, 351–355.
15 G. G. Zhanel and J. Q. Del Rosso, *J. Clin. Aesthetic Dermatol.*, 2016, **9**, 42.
16 H. Moustafa, M. A. Shemis, E. M. Ahmed and H. Isawi, *RSC Adv.*, 2024, **14**, 19680–19700.
17 L. Rojo, M. Fernandez-Gutierrez, S. Deb, M. M. Stevens and J. San Roman, *Acta Biomater.*, 2015, **27**, 32–41.
18 H. Moustafa, A. M. Karmalawi and A. M. Youssef, *Environ. Nanotechnol., Monit. Manage.*, 2021, **16**, 100482.
19 S. Y. Sung, L. T. Sin, T. T. Tee, S. T. Bee, A. R. Rahmat, W. A. W. A. Rahman, A. C. Tan and M. Vikhraman, *Trends Food Sci. Technol.*, 2013, **33**, 110–123.
20 N. A. Al-Tayyar, A. M. Youssef and R. Al-hindi, *Food Chem.*, 2020, **310**, 125915.
21 H. Moustafa, A. M. Youssef, N. A. Darwish and A. I. Abou-Kandil, *Composites, Part B*, 2019, **172**, 16–25.
22 H. M. C. Azeredo, C. G. Otoni, D. S. Corrêa, O. B. G. Assis, M. R. de Moura and L. H. C. Mattoso, *Biotechnol. J.*, 2019, **14**(12), 1900068.
23 H. Moustafa, N. El Kissi, A. I. Abou-Kandil, M. S. Abdel-Aziz and A. Dufresne, *ACS Appl. Mater. Interfaces*, 2017, **9**, 20132–20141.
24 Y. Yang, H. Liu, M. Wu, J. Ma and P. Lu, *Int. J. Biol. Macromol.*, 2020, **161**, 627–635.
25 L. Van Hai, E. S. Choi, L. Zhai, P. S. Panicker and J. Kim, *Int. J. Biol. Macromol.*, 2020, **144**, 491–499.
26 E. E. Okur, F. Eker, E. Akdaşçi, M. Bechelany and S. Karav, *Int. J. Mol. Sci.*, 2025, **26**, 9842.
27 Z. Yu, W. Wang, R. Dhital, F. Kong, M. Lin and A. Mustapha, *Colloids Surf., B*, 2019, **180**, 212–220.
28 A. Errokh, A. Magnin, J. L. Putaux and S. Boufi, *Mater. Sci. Eng., C*, 2019, **105**, 110044.
29 Z. Yu, W. Wang, F. Kong, M. Lin and A. Mustapha, *Int. J. Biol. Macromol.*, 2019, **129**, 887–894.
30 W. Wang, Z. Yu, F. K. Alsammarraie, F. Kong, M. Lin and A. Mustapha, *Food Hydrocolloids*, 2020, **100**, 105411.
31 H. Moustafa, S. F. Ibrahim, E. M. Ahmed and H. Atef, *J. Vinyl Addit. Technol.*, 2024, **30**, 855–867.
32 H. Moustafa, E. M. Ahmed, M. Hemida, M. Rabee and H. Isawi, *Diamond Relat. Mater.*, 2025, **157**, 112552.
33 H. Moustafa, H. Galliard, L. Vidal and A. Dufresne, *Eur. Polym. J.*, 2017, **87**, 188–199.
34 F. M. Abdel-Haleem, M. Hemida and H. Moustafa, *J. Adhes. Sci. Technol.*, 2025, **39**, 3099–3115.
35 B. Abderrahim, E. Abderrahman, A. Mohamed, T. Fatima, T. Abdesselam and O. Krim, *World J. Environ. Eng.*, 2015, **3**, 95–110.
36 H. Sadeghzadeh, A. Mehdipour, H. Dianat-Moghadam, R. Salehi, A. B. Khoshfetrat, A. Hassani and D. Mohammadnejad, *Stem Cell Res. Ther.*, 2022, **13**, 143.
37 D. D. S. Morais, D. D. Siqueira, C. B. B. Luna, E. M. Araujo, E. B. Bezerra and R. M. R. Wellen, Volume 6, Number 5,, *Mater. Res. Express*, 2019, **6**(5), 055315.
38 M. Rostami, G. Jahed-khaniki, E. M. aghaee, N. Shariatifar, M. A. Sani, M. Azami, S. Rezvantalab, S. Ramezani and M. Ghorbani, *Sci. Rep.*, 2024, **14**, 4372.
39 K. Shameli, M. Bin Ahmad, A. Zamanian, P. Sangpour, P. Shabanzadeh, Y. Abdollahi and M. Zargar, *Int. J. Nanomed.*, 2012, **7**, 5603–5610.
40 P. Khule, G. Lu, Q. Yang, R. Beaudry and E. Almenar, *Prog. Org. Coat.*, 2025, **207**, 109395.
41 Y. Liu, B. Sun, Z. Wang and Y. Ni, *BioResources*, 2016, **11**, 4226–4236.
42 X. Liu, X. Gu, J. Sun and S. Zhang, *Carbohydr. Polym.*, 2017, **167**, 356–363.
43 K. Jyoti, M. Baunthiyal and A. Singh, *J. Radiat. Res. Appl. Sci.*, 2016, **9**, 217–227.
44 H. Moustafa, S. Duquesne, B. Haidar and M. F. F. Vallat, *Polym. Compos.*, 2017, **38**, 966–973.
45 E. O. Mikhailova, *J. Funct. Biomater.*, 2020, **11**, 84.
46 H. Moustafa, S. M. El-Sayed and A. M. Youssef, *J. Thermoplast. Compos. Mater.*, 2023, **36**, 96–117.